CM² MAGAZINE

第 27 期

南方科技大学海洋磁学中心主编

创刊词

海洋是生命的摇篮，是文明的纽带。地球上最早的生命诞生于海洋，海洋里的生命最终进化成了人类，人类的文化融合又通过海洋得以实现。人因海而兴。

人类对海洋的探索从未停止。从远古时代美丽的神话传说，到麦哲伦的全球航行，再到现代对大洋的科学钻探计划，海洋逐渐从人类敬畏崇拜幻想的精神寄托演变成可以开发利用与科学研究的客观存在。其中，上个世纪与太空探索同步发展的大洋科学钻探计划将人类对海洋的认知推向了崭新的纬度：深海（deep sea）与深时（deep time）。大洋钻探计划让人类知道，奔流不息的大海之下，埋藏的却是亿万年的地球历史。它们记录了地球板块的运动，从而使板块构造学说得到证实；它们记录了地球环境的演变，从而让古海洋学方兴未艾。

在探索海洋的悠久历史中，从大航海时代的导航，到大洋钻探计划中不可或缺的磁性地层学，磁学发挥了不可替代的作用。这不是偶然，因为从微观到宏观，磁性是最基本的物理属性之一，可以说，万物皆有磁性。基于课题组的学科背景和对海洋的理解，我们对海洋的探索以磁学为主要手段，海洋磁学中心因此而生。

海洋磁学中心，简称 CM^2，一为其全名“Centre for Marine Magnetism”的缩写，另者恰与爱因斯坦著名的质能方程 $E = MC^2$ 对称，借以表达我们对科学巨匠的敬仰和对科学的不懈追求。

然而科学从来不是单打独斗的产物。我们以磁学为研究海洋的主攻利器，但绝不仅限于磁学。凡与磁学相关的领域均是我们关注的重点。为了跟踪反映国内外地球科学特别是与磁学有关的地球科学领域的最新研究进展，海洋磁学中心特地主办 CM^2 Magazine，以期与各位地球科学工作者相互交流学习、合作共进！

“海洋孕育了生命，联通了世界，促进了发展”。 21 世纪是海洋科学的时代，由陆向海，让我们携手迈进中国海洋科学的黄金时代

目 录

第 17 章　pTRM 检验真的管用吗?

根据以上讨论，各种影响因素排名最靠前的就是 PSD/MD 颗粒以及矿物转化的影响。

前人研究主要利用 pTRM 检验来核实到底有没有矿物转化的影响。pTRM 检验的最大特点在于实验流程简单，不需要太多额外的辅助实验就可以完成。pTRM 检验主要是在检查新矿物的 T_B 分布。

一般情况下，新生成的磁性矿物会有很宽泛的 T_B，也就是在高温和低温都有分布。比如，我们在 300-400°之间加热时，新生成矿物的 T_B 如果有低于 300°的，那么我们在做 200-300° TRM 检测时，就能发现确实存在矿物变化了。而且第二次的 pTRM（200°，300°）会比第一次的值要高。

可是问题在于，如果新生成的磁性矿物 T_B 比较高，都大于 400°，这个问题就比较麻烦了。对于这种情况，我们再回头检测 pTRM（200°，300°）时，就会发现没有新矿物出现，pTRM 检测通过!

但是，新生成的矿物已经存在，像病毒一样潜伏在高温段。只要我们的实验一来到高温段，它们就会发作，使得新获得的实验室 pTRM 值偏高，从而 Arai-plot 的高温段斜率变小，估算出来的地磁场古强度就会偏低。

如果高于当前加热温度，pTRM 检测无法胜任。

还有一种情况，更让人揪心。我们一直依赖的 Arai-plot 线性度也不完全可靠。如果没有矿物转化，SD 的 Arai-plot 肯定是一条笔直的斜线。可是，如果矿物转化是随着温度升高逐渐进行的，这会使得直线整体发生偏转，同时保持很好

的线性度，这种情况测量出来的古强度值会偏低。

另外一种情况是，原生磁性矿物被逐渐高温氧化，比如磁铁矿被逐渐氧化为磁赤铁矿，其 M_s 逐渐降低，相应的 pTRM 也会降低。这种影响会使得斜线向下偏转，斜率增大，从而高估地磁场古强度值。

这些情况我们很容易用现今喷发的熔岩流进行验证。对于过去几十年中喷发的熔岩流，我们确切知道它的发生时间以及地点，当然也就知道了已知的地磁场强度值。我们应用 Thellier 方法和 pTRM 检测来确定岩石记录的古地磁强度值，然后和已知值一对比，就知道很多样品并不能记录准确的强度值。

此时，我们就可以把古强度温度问题变为一个岩石磁学问题，我们需要回答这些通过了 pTRM 检验的样品为什么不能记录准确的强度值，能否通过这些样品提出新的判别标准，这可是一个非常前沿的科学问题。如果我们借此能够提出新标准，那么就可以自信地去研究地质历史时期中的岩石，构建地磁场古强度演化曲线，进而探讨地球深部的动力学过程。

比如，在检测加热过程中新生成的矿物时，pTRM 检测方法不总是很准，那么我们就得另外想办法。如果我们在实验过程中，单独准备一套样品（碎样边角料也可以），和古地磁样品同时加热，然后在室温测量其磁性变化，这些磁性包括磁化率、饱和等温剩磁以及非粘滞剩磁等等。如果有新矿物生成，无论其 T_B 是什么样的分布，室温参数都能把它们检测出来。当然，从实验角度来讲，会比 pTRM 检测复杂一些，多了一些实验成本，但是准确度大增。

SD 颗粒符合尼尔理论，是记录古地磁信息的良好载体。实践证明，PSD 颗粒也是古地磁的良好载体，但是其 Arai-plot 不是一条直线，不好拟合。在加热过程中，SD 颗粒由于粒径小，反而容易受到氧化作用，被改造。而 PSD 颗粒可

以较好地承受加热改造，性质反而更稳定。

这里面就出现了一个情况，如果样品确实是 PSD 颗粒占主导，该怎么去确定地磁场古强度呢？

我们可以取两块平行样品，其中一块在实验室中获得 TRM，与另外一块携带天然剩磁的样品一起做 Thellier-Thellier 实验，这样就获得了两条 Arai-plot 曲线。然后我们把天然剩磁的曲线用实验室 TRM 的曲线进行归一化，这样就会得到一条较为笔直的 Arai-plot 行为，经过证实，其斜率就可用来计算地磁场古强度。

除了以上的各种处理，当属 John Tarduno 教授的独门绝技最为特别。他发现大部分的加热改造行为都和样品的基质（Matrix）有关。于是，他就发明了单晶技术，把火山岩里结晶的大颗粒单晶挑选出来，进行古强度实验。这些单晶体积不大，于是他就把超导磁力仪的磁探头缩小，提高了测量精度。所以，目前全世界的古地磁实验室，只有 Tarduno 教授拥有这样的小磁探头超导磁力仪，也只有他的实验室能够进行单晶实验。

拥有了这项神奇的技术，Tarduno 教授的实验室成果颇丰，得出了与以往不大相同的结论。

比如，对白垩纪超静磁（CNS）的地磁场古强度研究中，前人一般认为地磁场强度很低。Lisa Tauxe 教授还专门挑选了海底玄武岩表层玻璃（含有大量 SD 颗粒）进行测量，也得出 CNS 期间地磁场古强度是低的。Tarduno 教授利用单晶测量，发现 CNS 期间地磁场古强度应该是高的，于是就产生了一定的观点分歧。

大家会问刘老师你的观点如何？

如前所述，我们的学科组目前正在进行详细的岩石磁学实验，研究近期熔岩流记录地磁场强度的能力及判别标准，然后再对这些古老的岩石重新进行测量。

除此之外，我们也另辟新径，用多介质相互验证的方式来进行研究。

除了喷发出来的熔岩流，海底洋壳也记录了统一时期的地磁场信息。沉积物通过沉积物剩磁（Depositional remanent magnetization，DRM）从另外一个角度记录了地磁场强度的相对变化。我们的整体思路是，同时研究者三种不同的介质，看看它们记录的强度变化特征是否一致。如果三种独立的方法都显示类似的变化特征，我们就可以自信地确定地磁场古强度的变化模式。

文献导读

1. 地核是水的储库

翻译人：冯婉仪 fengwy@sustech.edu.cn

Li Y G, Vočadlo L, Sun T, et al. ***The Earth ' s core as a reservoir of water****[J].* ***Nature geoscience****, 2020, 13: 453-458.*

摘要：目前对地球上水的含量和分布的估算有很大的不确定性，其中大部分原因是由于缺乏关于地球深部的信息。最近的研究表明，地球可能在其演化的早期阶段从富含氢的太阳星云中获得了大量的水，并且地球大量的水可能已经进入到地核中。在这里，我们使用从头算分子动力学和热力学集成技术计算了在 20-135 GPa 和 2,800-5,000 K 条件下，水在铁和硅酸盐熔体之间的分配系数。结果表明，在地核-地幔分异和地核-地幔边界条件下，水的亲铁性随温度的升高而减弱。然而，我们发现在地核形成条件下，在还原和氧化的情况下，水总是强烈地分配进入到铁液中。通过计算氢在平衡的铁和硅酸盐熔体之间的分布的经验计数法也验证了水的亲铁性。因此，我们得出结论，地核可能扮演一个大型水储库的角色，它包含了地球上大部分的水。除了对挥发份输送的吸积模型有约束，这些发现可能部分地解释了由测量的地震速度所隐含的地核低密度的原因。

ABSTRACT: Current estimates of the budget and distribution of water in the Earth have large uncertainties, most of which are due to the lack of information about the deep Earth. Recent studies suggest that the Earth could have gained a considerable amount of water during the early stages of its evolution from the hydrogen-rich solar nebula, and that a large amount of the water in the Earth may have partitioned into the core. Here we calculate the partitioning of water between iron and silicate melts at 20-135 GPa and 2,800-5,000 K, using ab initio molecular dynamics and thermodynamic integration techniques. Our results indicate a siderophile nature of water at core–mantle differentiation and core-mantle boundary conditions, which weakens with increasing temperature; nevertheless, we found that water always partitions strongly into the iron liquid under core-formation conditions for both reducing and oxidizing scenarios. The siderophile nature of water was also verified by an empirical-counting method that calculates the distribution of hydrogen

in an equilibrated iron and silicate melt. We therefore conclude that the Earth's core may act as a large reservoir that contains most of the Earth's water. In addition to constraining the accretion models of volatile delivery, the findings may partially account for the low density of the Earth's core implied by measured seismic velocities.

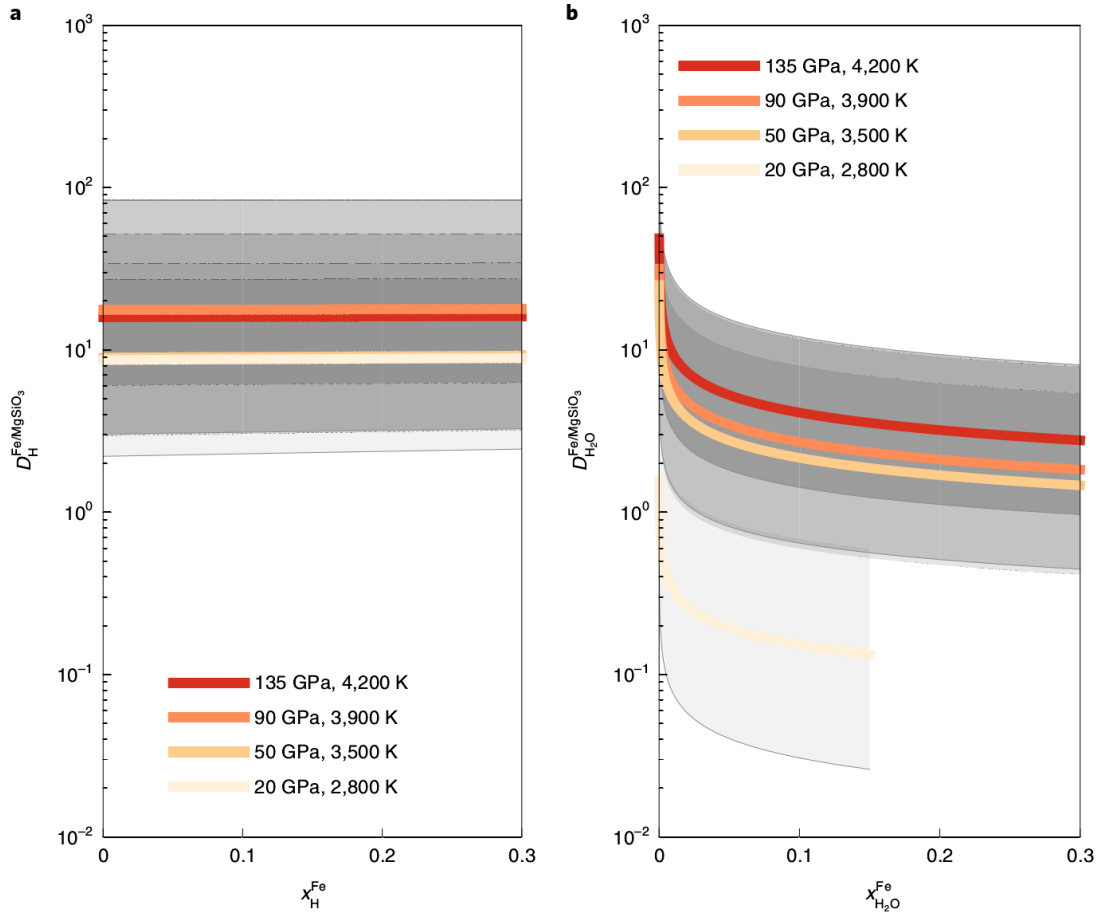

Figure 1. Partition coefficient. a,b, Derived partition coefficients between the iron and silicate melts as a function of concentration in iron for H (a) and H_2O (b). Shaded regions indicate the uncertainties. Supplementary Information gives a better view with uncertainties.

2. 残留在东地中海的中生代洋壳

翻译人：李园洁 liyj3@sustech.edu.cn

Granot R. ***Palaeozoic oceanic crust preserved beneath the eastern Mediterranean[J]. Nature Geoscience****, 2016, 9(9): 701-705.*

摘要：洋壳俯冲到地幔使得现在的洋盆年龄相对年轻，从而阻碍我们认识古老大洋岩石圈。但存在一个例外，东地中海（包括西多罗的盆地和黎凡特盆地）保存有新特提斯洋或更老洋盆的南缘。异常厚的沉积层和缺乏准确的磁异常数据导致对其洋壳的性质和年龄一直存在争议。本文分析了西多罗的盆地的总的和矢量磁异常数据，识别出一个长的线性磁异常序列，表明地壳是大洋来源。作者利用这些磁异常的形状或偏斜度来约束洋壳形成的时间，推测形成时间为~ 340 Ma。这些洋壳可能沿着特提斯扩张系统形成，这意味着新特提斯洋的形成比先前想象的更早，或者是在潘基亚超大陆融合过程中形成。最后在黎凡特盆地发现的薄且伸展的陆壳向相对厚的西多罗的洋壳的过渡可以指导现今的地震活动模式和该地区的板块构造运动。

ABSTRACT: Subduction of oceanic crust into the mantle results in the relatively young Mesozoic–Cenozoic age of the current oceanic basins, thus, hindering our knowledge of ancient oceanic lithospheres. Believed to be an exception, the eastern Mediterranean Sea (containing the Herodotus and Levant basins) preserves the southern margin of the Neotethyan, or older ocean. An exceptionally thick sedimentary cover and a lack of accurate magnetic anomaly data have led to contradicting views about its crustal nature and age. Here I analyse total and vector magnetic anomaly data from the Herodotus Basin. I identify a long sequence of lineated magnetic anomalies, which imply that the crust is oceanic. I use the shape, or skewness, of these magnetic anomalies to constrain the timing of crustal formation and find that it formed about 340 million years ago. I suggest that this oceanic crust formed either along the Tethys spreading system, implying the Neotethys Ocean came into being earlier than previously thought, or during the amalgamation of the Pangaea Supercontinent. Finally, the transition from the rather weak and stretched continental crust found in the Levant Basin to the relatively strong oceanic Herodotus crust seems to guide the present-day seismicity pattern as well as the plate kinematic evolution of the region.

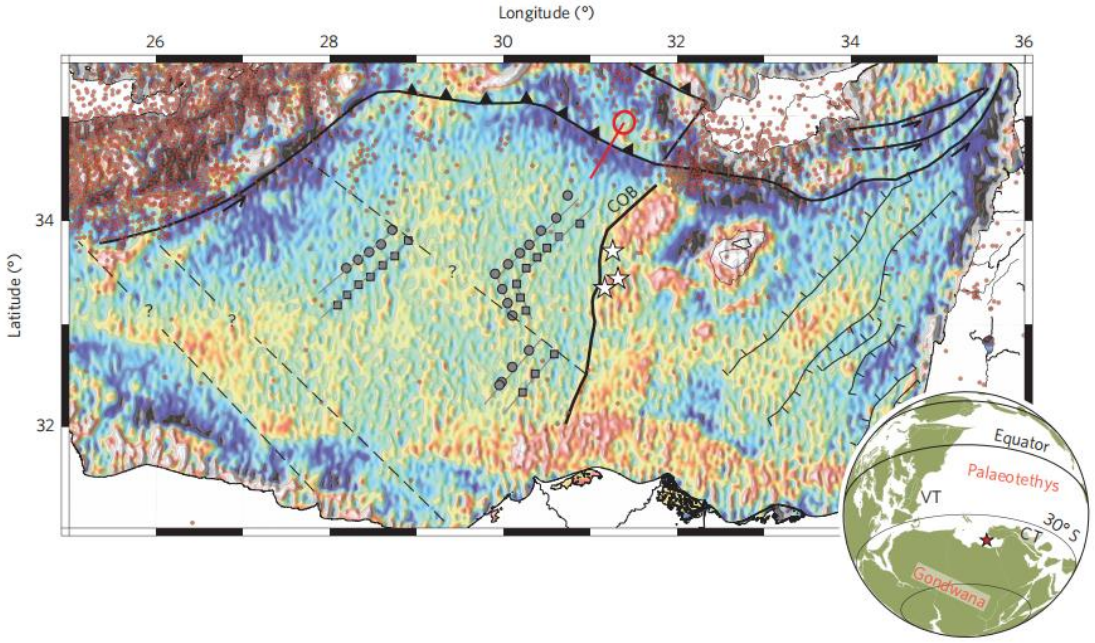

Figure 1. Tectonic map of the eastern Mediterranean. Background is a VGG map. Boundaries of basement highs in the Levant Basin are based on a Bouguer map and on seismic data. White-filled stars show the transition between two- and three-dimensional magnetic source layers computed along vector profiles. Grey-filled symbols denote isochrons. The dashed lines delineate the suspected location of fracture zones based on magnetic anomaly offsets and the background gravity grid. The motion of the Nubia Plate relative to that of the Anatolia Plate is shown across the Cyprus arc with a red line (16.2 mm/yr). Red dots denote earthquake epicentres taken from the USGS catalogue with body wave magnitude (m_b)>3 between 1972 and 2015. The inset panel shows the 340 Myr global palaeogeographic reconstruction. Red star delineates the location of the Herodotus Ridge. Abbreviations: COB, continent-ocean boundary; VT, Variscan Terranes; CT, Cimmerian Terranes.

3. 古新世-始新世极热期间海洋萧条与呼吸作用使碳酸盐溶解增强

翻译人：蒋晓东 jiangxd@sustech.edu.cn

Ilyina, T., and Mathia,s H. (2019). ***Carbonate Dissolution Enhanced by Ocean Stagnation and Respiration at the Onset of the Paleocene-Eocene Thermal Maximum****. Geophysical Research Letters. 46, 2, 842-852.*

摘要：古新世-始新世的极热现象是碳诱导全球暖化的短暂事件，该事件被认为类似于当前气候变化。多项古环境指标表明古新世-始新世极热初期底层水减少，然而其对古环境的影响并不清楚。基于地球系统模型研究，本研究发现大洋翻转流的变化是海洋脱氧和碳酸盐溶解的关键。气候暖化驱动了南大洋底层水减弱和大洋海水分层增强，引起大西洋和太平洋海盆尺度碳酸盐溶解的不同步。减弱的大洋通风引起中层水再次矿化产物（二氧化碳和营养盐）的聚集，因此降低了氧气含量但增加了二氧化碳含量。这就触发了整个水团中碳酸盐的溶解，而大洋表层仍然是饱和的。本研究的发现有助于理解碳循环对气候变化长时间尺度响应。

ABSTRACT： The Paleocene-Eocene Thermal Maximum was a transient, carbon-induced global warming event, considered the closest analog to ongoing climate change. Impacts of a decrease in deepwater formation during the onset of the Paleocene-Eocene Thermal Maximum suggested by proxy data on the carbon cycle are not yet fully understood. Using an Earth System Model, we find that changes in overturning circulation are key to reproduce the deoxygenation and carbonate dissolution record. Weakening of the Southern Ocean deepwater formation and enhancement of ocean stratification driven by warming cause an asymmetry in carbonate dissolution between the Atlantic and Pacific basins suggested by proxy data. Reduced ventilation results in accumulation of remineralization products (CO_2 and nutrients) in intermediate waters, thereby lowering O_2 and increasing CO_2. As a result, carbonate dissolution is triggered throughout the water column, while the ocean surface remains supersaturated. Our findings contribute to understanding of the long-term response of the carbon cycle to climate change.

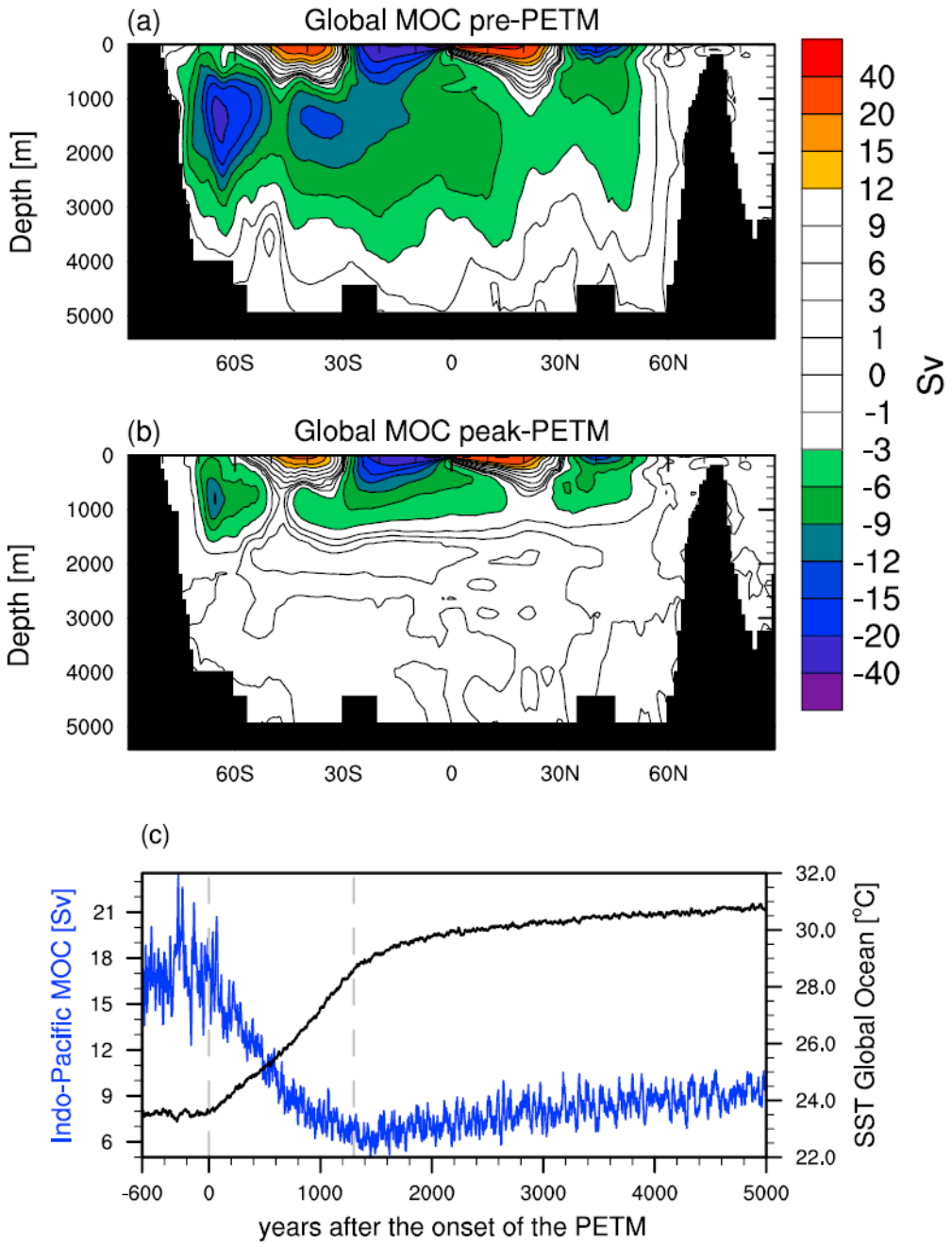

Figure 1. Response of the meridional overturning circulation and sea surface temperature to PETM warming. (a) Stream function of the globally averaged MOC (Sv) for the pre-PETM setting. Positive values correspond to clockwise circulation. (b) Globally averaged MOC at the end of the PETM simulation (mean over last 30 simulation years). (c) Time series of the South Pacific MOC (absolute values, 10-year running mean, blue line) and the global SST (black line) over the whole experiment. Negative years refer to the pre-PETM background state. Dashed gray lines indicate the beginning and termination of atmospheric CO_2 increase, respectively. PETM = Paleocene-Eocene Thermal Maximum; MOC = Meridional Overturning Circulation; SST = sea surface temperature.

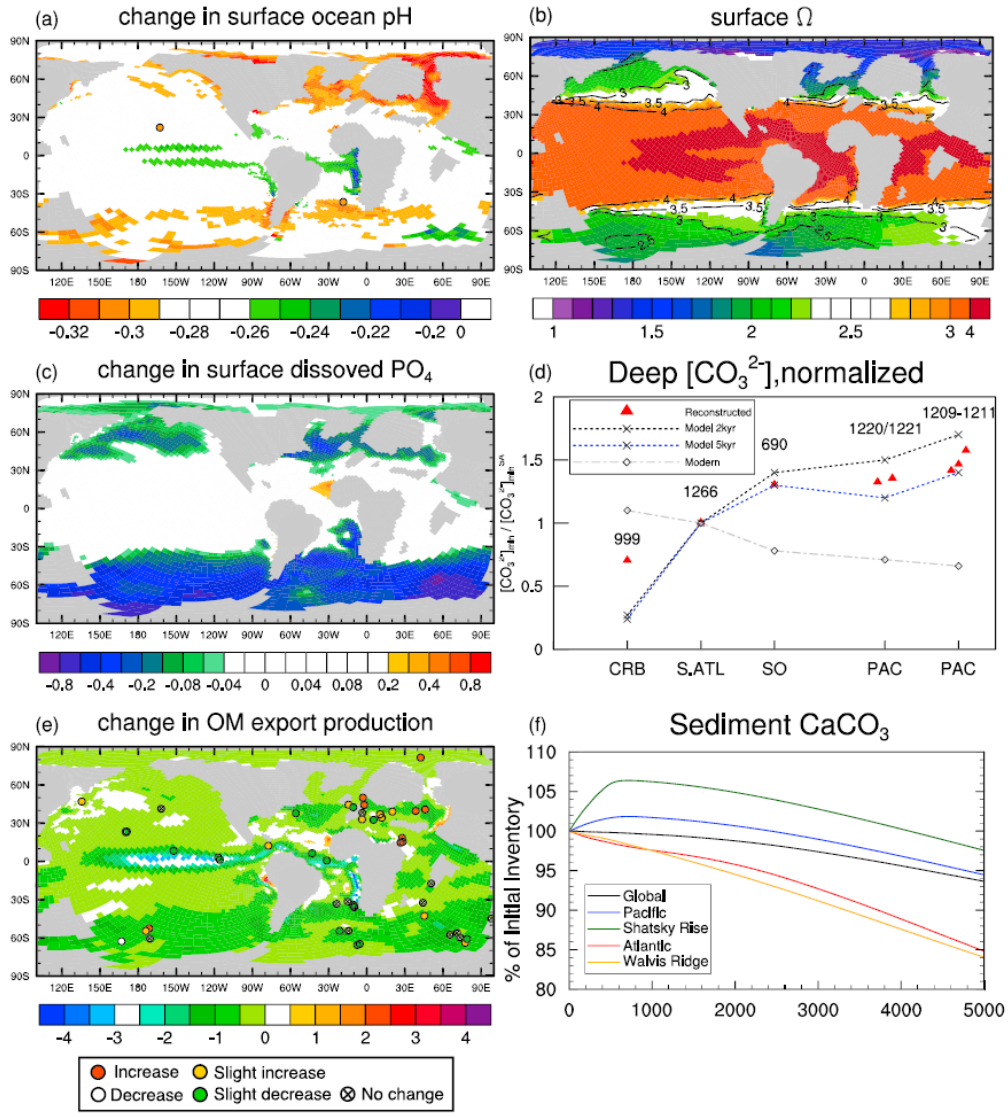

Figure 2. Changes in ocean biogeochemistry at the sea surface, in the deep ocean and sediments. (a) Anomaly (calculated as difference between peak PETM and pre-PETM state) in surface pH, overlain with pH reconstructions (Penman et al., 2014). (b) Surface distribution of calcite saturation state (Ω, mean over the last 30 simulation years). Contour lines show surface Ω of the pre-PETM background state. (c) Anomaly in surface dissolved phosphate (PO_4, µmol/L). (d) Simulated deep-sea CO^{2-}_3 basin gradient at 2 and 5 kyr after the onset of the PETM and reconstructions (Zeebe & Zachos, 2007), both based on site-specific minimum [CO^{2-}_3] normalized to S.ATL site. CRB = Caribbean; S.ATL = South Atlantic Ocean; SO = Southern Ocean, PAC = Pacific Ocean. (e) Anomaly in export production (mol C · m-2 · year-1), overlain with productivity tendencies from reconstructions (Winguth et al., 2012). (f) Change in $CaCO_3$ sediment content over the whole sediment depth of the model (percent of pre-PETM inventory) for specific regions. Shatsky Rise and Walvis Ridge region are defined in supporting information Figure S5. Note the nonlinear color scales in subplots (c) and (b). PETM = Paleocene-Eocene Thermal Maximum; OM = organic matter.

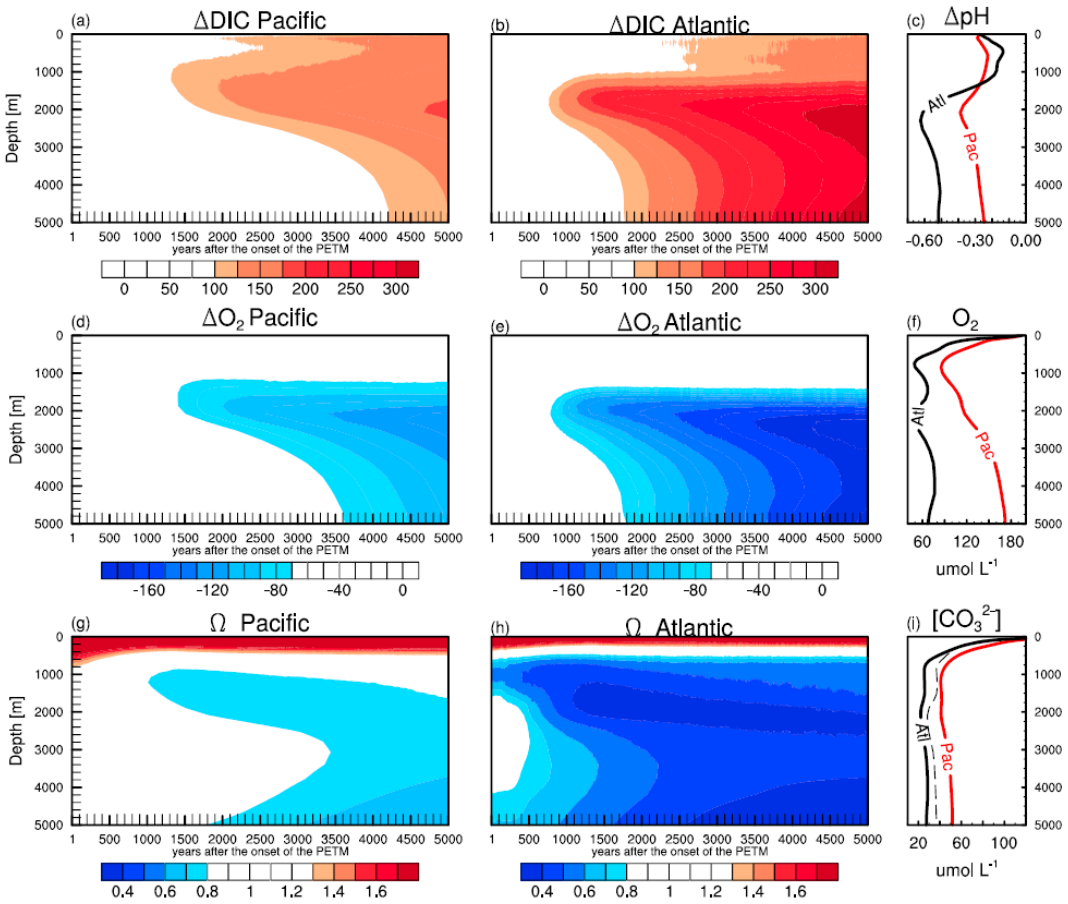

Figure 3. Ocean biogeochemistry response to biological respiration processes in a poorly ventilated ocean of the PETM. Temporal evolution of DIC anomaly averaged over (a) the Pacific and (b) the Atlantic basin. (c) Depth profile of pH anomaly (peak PETM and pre-PETM) averaged over the Pacific (red line) and the Atlantic Oceans (black line). Temporal evolution of oxygen (O_2) anomaly averaged over (d) the Pacific and (e) the Atlantic basins. (f) Depth profiles of oxygen concentration (mean over last 30 simulation years). Temporal evolution of Ω averaged over (g) the Pacific and (h) the Atlantic basins. (i) Depth profile of [CO^{2-}_3]; dashed line indicates South Atlantic [CO^{2-}_3]. All concentrations are given in micromole per liter. PETM = Paleocene-Eocene Thermal Maximum; DIC = dissolved inorganic carbon.

4. 中国东海北部过去四十万年的古海洋变迁：来自 IODP U1429 孔放射虫组合变化的指示

翻译人：杨会会 11849590@mail.sustech.edu.cn

Matsuzaki K M, Itaki T, Tada R. ***Paleoceanographic changes in the Northern East China Sea during the last 400 kyr as inferred from radiolarian assemblages (IODP Site U1429)[J]. Progress in Earth and Planetary Science,*** *2019, 6:22*

摘要：中国东海是一个浅边缘海，对冰期海平面变化敏感，在东亚夏季风盛行季节受温暖而贫营养的黑潮、温暖而营养丰富的台湾暖流和华南河流输入淡水的共同影响。由于海床的高沉积速率，这一区域 40 ka 以前的古海洋变化研究仍然较少。在 IODP 346 航次期间，中国东海北部 U1429 点位钻取了涵盖过去 400 kyr 的长沉积岩心。这些岩心含有大量保存良好的放射虫，因此本文利用其生态特征分析了冰期海平面变动是如何影响过去 400 kyr 中国东海的古海洋状态，并关注了中间层海水性质的变化。此外，通过分析特定放射虫种属数据的方式，本文确定了夏季表层海水温度和 500 米中间层海水温度。尽管直到间冰期 MIS 1 和 5 海平面出现高值之后黑潮向中国东海的涌入很可能被延缓了，但是在过去 400 kyr 的每一个间冰期时期（即 MISs 1、5、7、9 和 11 期间），U 1429 点位的浅层海水都受到了黑潮影响，并进而导致了一个高夏季表层海水温度（约 27℃）的状态。在这一延缓时期，中国东海大陆架水体对其的影响占据了主导。在冰期 MISs 2-4、6 和 10 期间，本文数据表明海岸带条件占据了相应的主导地位，很可能是超过 90 米的海平面下降引起的。这一时期，夏季海水表层温度更冷，约为 20℃。*Cycladophora davisiana* 种属相对数量的变化指示了在 MIS 6 期间底层水发生了最为显著的变化，当时底层水很可能更为缺氧。在 MISs 7 和 6 期间，浅层水初级生产力的提升可能是引起其贫氧状态的关键原因。

ABSTRACT: The East China Sea (ECS) is a shallow marginal sea that is sensitive to glacio-eustatic sea-level changes and is influenced by warm oligotrophic water of the Kuroshio Current (KC), the nutrient-rich Taiwan Warm Current, and freshwater discharges from rivers in southern China during the East Asian summer monsoon season. In this area, local paleoceanographic changes for times prior to 40 ka remain poorly studied because of high sediment accumulation rates on the seafloor. During Integrated Ocean Drilling Program Expedition 346, long sediment cores representing the last 400 kyr were retrieved from the northern part of the ECS (Site U1429). In these cores,

radiolarians are abundant and well-preserved, thus using the ecological properties of radiolarians, we analyzed how glacio-eustatic sea-level variations have influenced the paleoceanography of the ECS over the last 400 kyr, with a focus on changes in water properties at intermediate depths. Additionally, the summer sea surface temperature (SST) and intermediate water temperature at about 500 m were quantified by means of data on selected radiolarian species. The KC influenced the shallow water at Site U1429 during each interglacial period over the last 400 kyr (marine isotope stages [MISs] 1, 5, 7, 9, and 11), causing a high summer SST (about 27 °C), although inflow of the KC into the ECS was probably delayed until after the sea-level maximum of interglacial MIS 1 and MIS 5. During this lag time, ECS shelf water was the dominant influence on the system. During glacial periods (MISs 2–4, 6, and 10), our data suggest that coastal conditions prevailed, probably because of a sea-level drop of more than 90 m. At these times, the summer SST was colder, ca. 20 °C. Changes in the relative abundance of Cycladophora davisiana indicate that the most significant changes in the bottom water occurred during MIS 6, when the bottom water likely became poorer in oxygen. An increase in the shallow-water primary productivity during MIS 7 and MIS 6 was probably the key factor causing the oxygen-poor conditions.

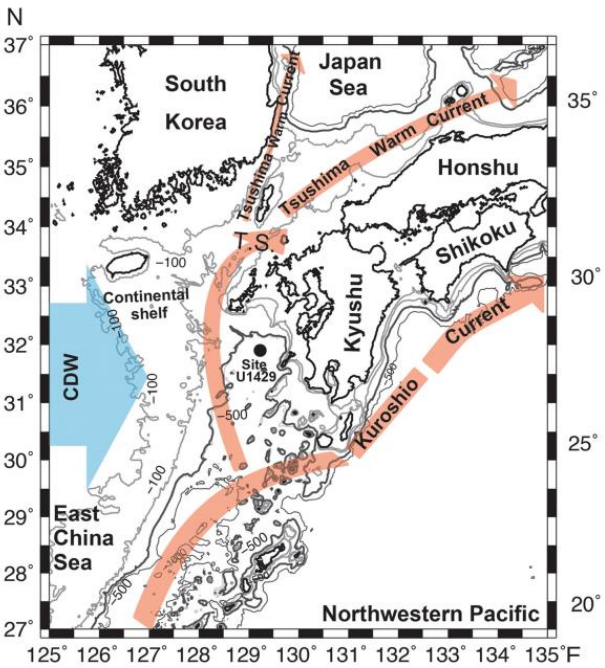

Figure 1. Map from Matsuzaki et al. (2016) modified for this study to show the location of site U1429 and the key oceanographic features of the study area. CDW means Changjiang diluted water and IODP means Integrated Ocean Drilling Program (Sample 346-U1429A-7H6-27-29 cm); 26 Dimelissa thoracites (Haeckel) (sample 346-U1429A-1H1-27-29 cm); 25 Phormacantha hystrix Jørgensen.

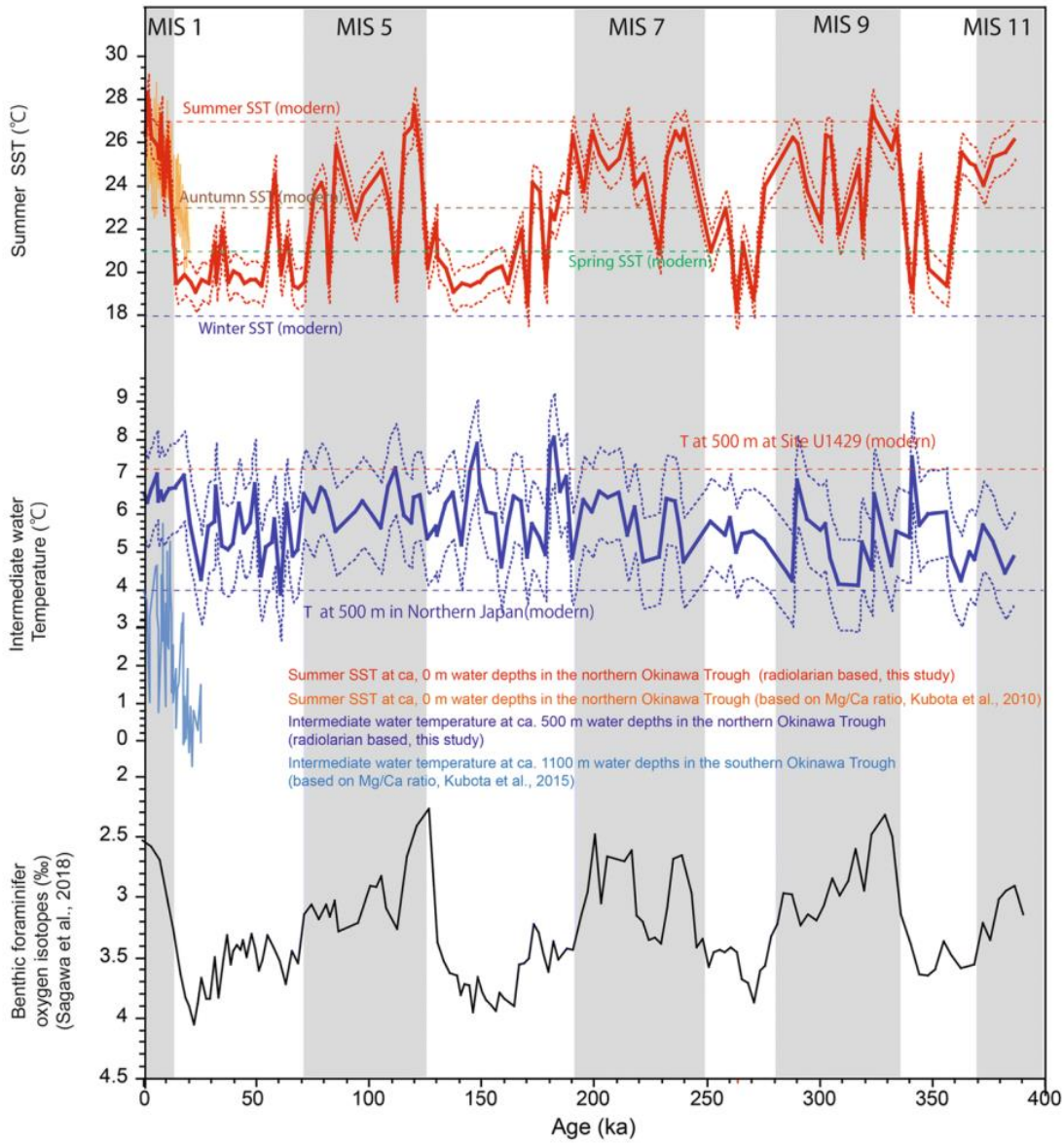

Figure 2. Radiolarian-based estimates for intermediate water temperature and SST over time and compared to the benthic foraminifera isotope curve of Sagawa et al. (2018). Dashed curves indicate modern median temperatures. Also shown are the summer SST estimated using the Mg/Ca ratio of planktic foraminifera (Kubota et al. 2010) in the northern Okinawa Trough and bottom water temperature estimated using the Mg/Ca ratio of benthic foraminifera in the southern Okinawa Trough (Kubota et al. 2015b)

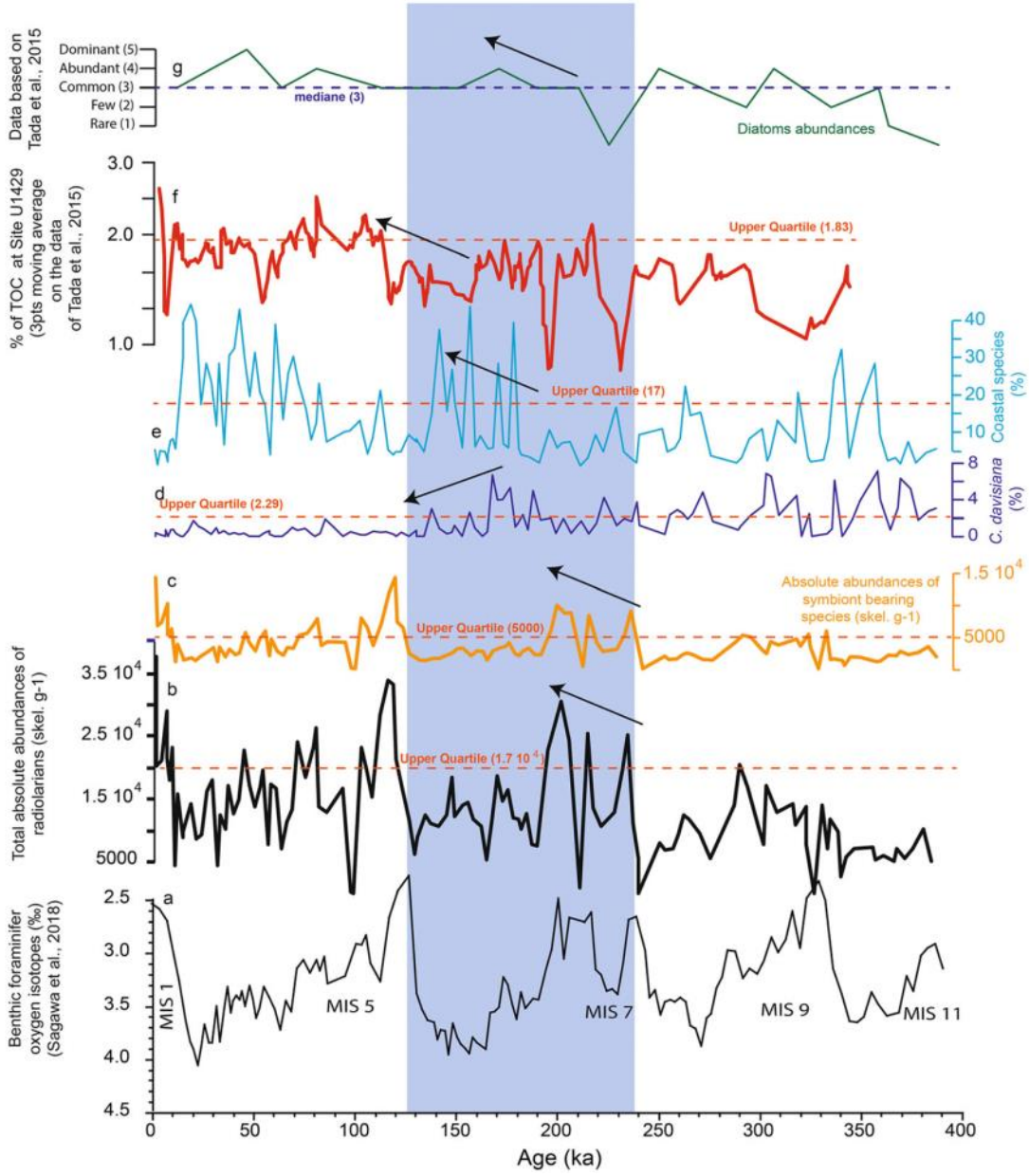

Figure 3. Temporal fluctuation of the local primary productivity: a benthic foraminifera isotope curve of Sagawa et al. (2018), b radiolarian absolute abundance, c radiolarian absolute abundance of species bearing algal symbiosis based on Zhang et al. 2018 (A. vinculata, B. scutum, L. hispida, P. obeliscus, P. praetextum, P. clausus, A. lappacea/spinosa, D. tetrathalamus, D. muelleri, P. pylonium group, S. resurgens, S. streptacantha, Tetrapyle circularis/fruticosa group, L. reticulata, Heliodiscus spp., D. elegans), d C. davisiana (%), e continental shelf species (%), f total organic carbon (TOC)(%), and g diatom abundances.

5. 天文调谐作用控制着过去 160 千年西太平洋暖池区表层和温跃层的变化

翻译人：仲义 zhongy@sustech.edu.cn

M. Hollstein, M. Mohtadi, M. Kienast, et al., ***The impact of Astronomical forcing on surface and thermocline variability within the western Pacific Warm Pool over the past 160 kyr*** *[J]. Paleoceanography and Paleoclimatology 2020,35, 6, e2019PA003832 12673.*

https://doi.org/10.1029/2019PA003832

摘要：西太平洋暖池区（WPWP）通过提供全球大气热量和湿度来调控全球气候系统。然而，过去西太平洋暖池的古海洋学与气候学变化仍然存在争议。因此，作者整合最新和过去发表的西太平洋暖池区赤道南北两侧的表层和温跃层的和海水中氧同位素结果，发现天文调谐作用在冰期-间冰期起到关键性作用。我们发现在过去 160 千年以来 WPWP 南北两侧所有记录表现出明显的一阶一致性特征，表明暖池区空间分布结构相对稳定。同时区域性变化又直接影响二阶的变异性。在西太平洋暖池海域，降水变化均匀。温跃层记录表明南北太平洋地区水团对 WPWP 的影响作用。温跃层温度的差异归因于不同的斜率作用对不同站位温跃层水团的影响。而岁差作用对 WPWP 地区南北部温跃层均有影响，在岁差带上温跃层条件的变化归因于温跃层水团来源的改变、区域性大气环流的变化以及 ENSO 的综合作用。

ABSTRACT: The Western Pacific Warm Pool (WPWP) constitutes an important component within the global climate system by providing an enormous amount of heat and moisture to the global atmosphere. Nevertheless, past variability of oceanography and climate across the WPWP is still debated. Here, we compile newly generated and published surface and thermocline temperature and seawater stable oxygen isotope (δ^{18}OSW) records from the WPWP north and south of the equator to monitor its variability, particularly in response to astronomical forcing, over the last glacial - interglacial cycle. We find a coherent first - order variability in all records from the northern and southern WPWP sites over the past 160 kyr indicating a relatively stable WPWP spatial structure. The second - order variability is modulated by regionally varying influences. Precipitation varied uniformly across the WPWP marine realm. Thermocline records illustrate the influence of both northern and southern Pacific waters on the WPWP. Differences between the thermocline temperature records are attributed to the differing effect of obliquity on the thermocline water masses influencing the individual

sites. Precession exerts an influence on the thermocline at both northern and southern WPWP sites. Variations in thermocline conditions in the precession band are attributed to a combination of modifications in the thermocline source waters, changes in the regional atmospheric circulation and the El Niño‐Southern Oscillation regime.

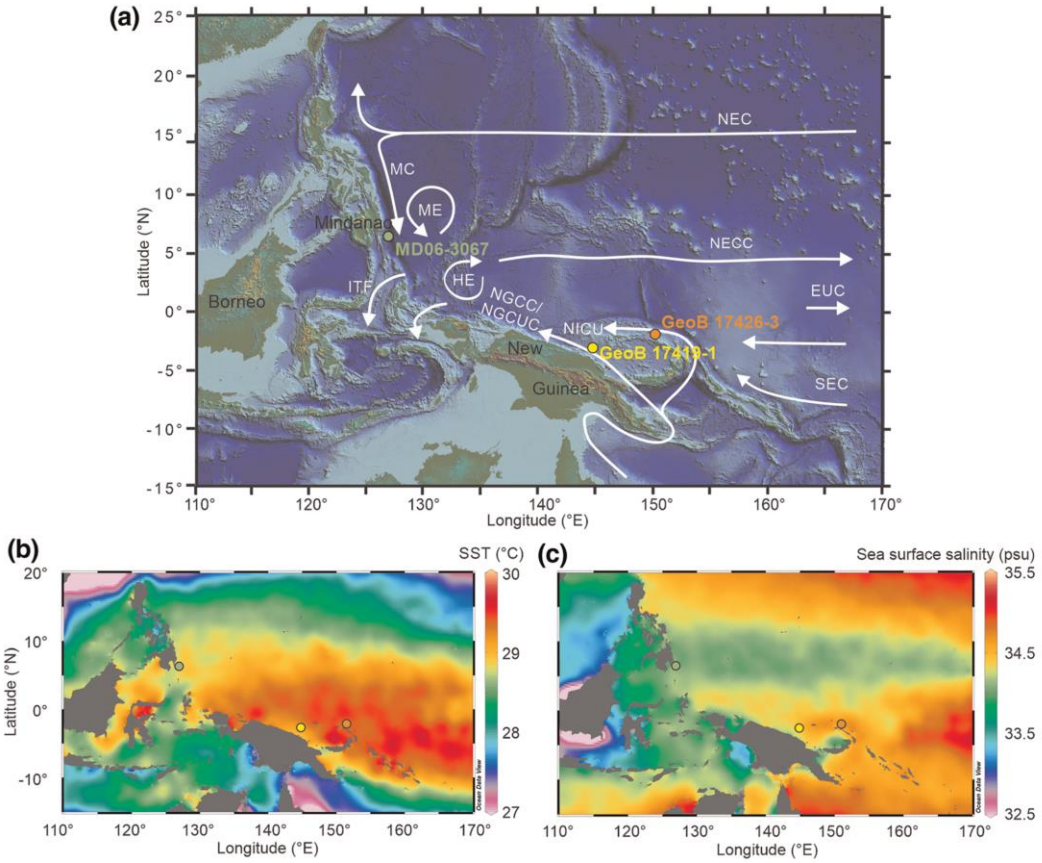

Figure 1. (a) Bathymetric map of the study area. White arrows schematically indicate the main (sub)surface currents that influence the WPWP. EUC = Equatorial Undercurrent; ITF = Indonesian Throughflow; MC = Mindanao Current; NEC = North Equatorial Current; NECC = North Equatorial Counter Current; NGCC = New Guinea Coastal Current; NGCUC = New Guinea Coastal Undercurrent; SEC = South Equatorial Current. The position of gravity core GeoB 17426‐3 (this study) is indicated by an orange dot. Core GeoB 17419‐1 (Hollstein et al., 2018) is a reoccupation of core MD05‐2920 (Tachikawa et al., 2014) both marked by a yellow dot. MD06‐3067 (Bolliet et al., 2011) is marked by a green dot. (b) Annual sea surface temperatures and (c) sea surface salinity across the WPWP (Locarnini et al., 2013; Zweng et al., 2013). The temperature and salinity maps were generated using the Ocean Data View software (Schlitzer, 2014).

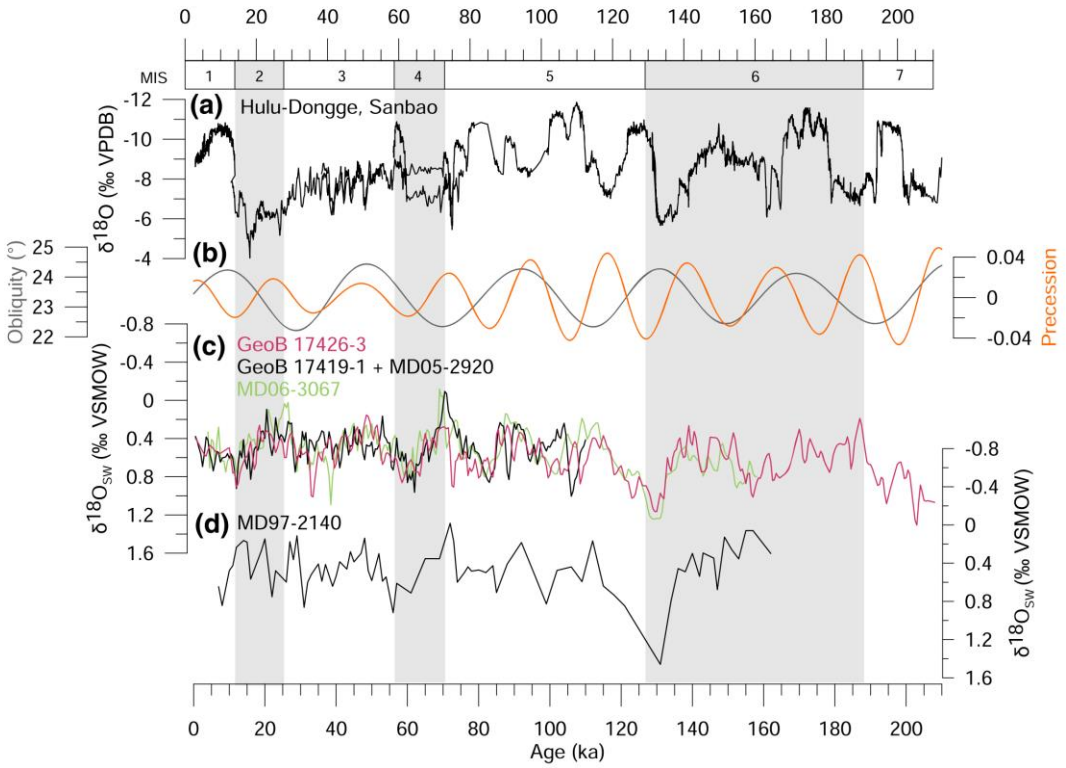

Figure 2. Comparison of rainfall records from the WPWP marine realm and eastern China. (a) Speleothem δ18O records from the Hulu‐Dongge and Sanbao caves in eastern China (Wang et al., 2001; Wang et al., 2008). (b) Variations in obliquity (gray) and precession (orange). (c) δ18OSW of GeoB 17426‐3 (this study), combined MD05‐2920 and GeoB17419 (Hollstein et al., 2018; Tachikawa et al., 2014), and MD06‐3067 (Bolliet et al., 2011). For consistency all records were resampled on intervals of 0.5 ka. (d) δ18OSW of MD97‐2140 (de Garidel‐Thoron et al., 2005). Marine isotope stages are indicated at the top. MIS 6, 4, and 2 are marked by gray.

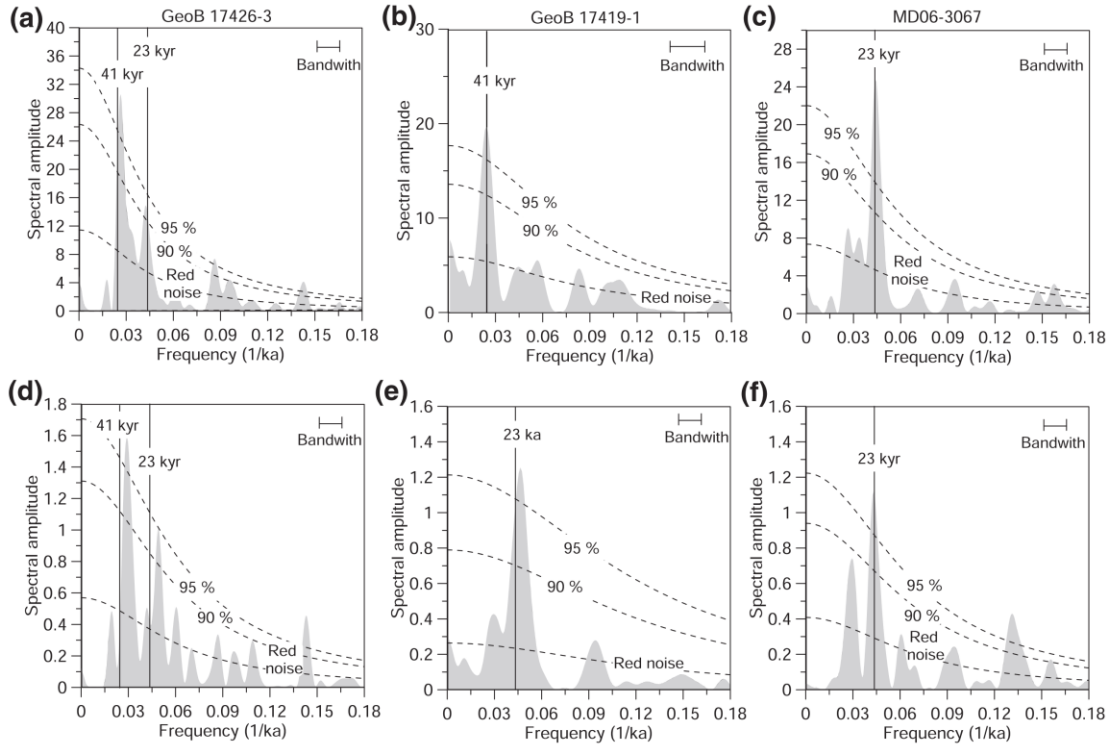

Figure 3. Spectra of thermocline temperature (a–c) and δ18OSW (d–f) of GeoB 17426‐3(a and d), GeoB 17419‐1 (b and e), and MD06‐3067 (c and f). Spectral analyses were performed using REDFIT (e.g., Schulz & Mudelsee, 2002). We eliminated frequencies below 0.018 kyr-1 from the records to exclude glacial‐interglacial variations from the analyses. We chose a Welch type spectral window and used an oversampling factor of 9. The bandwidth is 6 dB. Dashed lines denote the red‐noise spectrum and 90% and 95% confidence levels. Vertical black bars indicate frequencies that correspond to the periodicities of precession (23 kyr) and obliquity (41 kyr).

6. 泰国柚木 338 年树轮氧同位素记录捕获了亚洲夏季风系统变化

翻译人：郑威　11930589@mail.sustech.edu.cn

Pumijumnong N, Bräuning A, Sano M, et al. ***A 338-year tree-ring oxygen isotope record from Thai teak captures the variations in the Asian summer monsoon system****[J].* ***Scientific Reports****, 2020, 10(1): 1-11.*

摘要：文章展示了一个从泰国西北部Mae Hong Son省采集的一个柚木树轮纤维素338年氧同位素记录。这个树轮序列保存了区域性湿润季节降雨和相对湿度的同位素信号。树轮氧同位素与五月到十月的区域性降雨有强相关关系，显示了东南亚地区大区域的一致变化。作者基于线性回归模型重建了夏季风季节性降雨。空间相关关系和频谱分析揭示了ENSO对树轮氧同位素记录有很大的影响。在印度夏季风较弱的时期ENSO对树轮氧同位素记录的影响会更明显。

ABSTRACT：A 338-year oxygen isotope record from teak tree-ring cellulose collected from Mae Hong Son province in northwestern Thailand was presented. The tree-ring series preserves the isotopic signal of the regional wet season rainfall and relative humidity. Tree-ring $\delta^{18}O$ correlates strongly with regional rainfall from May to October, showing coherent variations over large areas in Southeast Asia. We reconstructed the summer monsoon season (May to October) rainfall based on a linear regression model that explained 35.2% of the actual rainfall variance. Additionally, we found that in the 19th century, there was a remarkable drought during many years that corresponded to regional historic drought events. The signals of the June to September Indian summer monsoon (ISM) for the period between 1948 and 2009 were clearly found. Spatial correlations and spectral analyses revealed a strong impact of the El Niño-Southern Oscillation (ENSO) on tree-ring $\delta^{18}O$. However, ENSO influenced the tree-ring $\delta^{18}O$ more strongly in the 1870–1906, 1907–1943, and 1944–1980 periods than in the 1981–2015 period, which corresponded to periods of weaker and stronger ISM intensity.

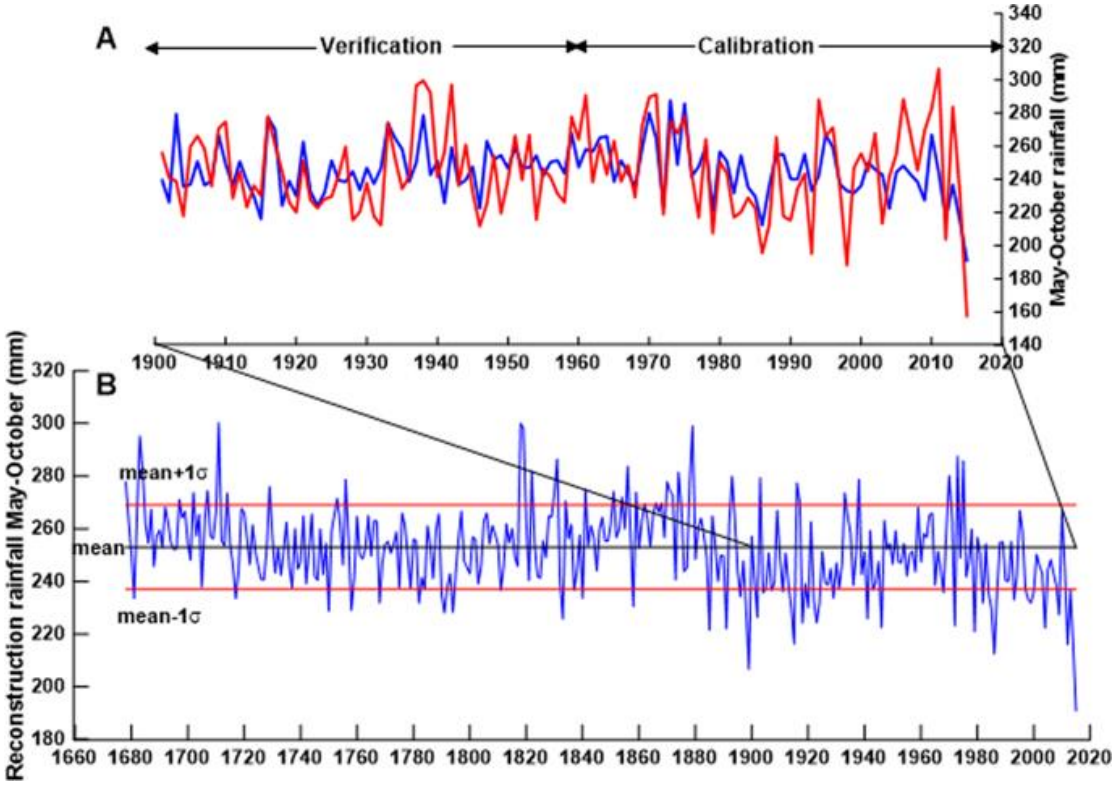

Figure 1. May to October rainfall (mm), red line is actual CRU TS4.03 rainfall (mm) and blue line is reconstruction May-October rainfall (mm) (**A**), reconstruction rainfall May–October black line is the average rainfall of 253 mm, read line (mean + 1σ) is 269 mm, and (mean − 1σ) is 237 mm (**B**).

7. 中新世火灾加剧与青藏高原持续干旱化的联系

翻译人：曹伟

Miao Y, Wu F, Warny S, et al. ***Miocene fire intensification linked to continuous aridification on the Tibetan Plateau****[J].* ***Geology****, 2019, 47(4): 303-307.*

摘要：虽然火灾被认为是全球植被演变和气候变化的重要因素，但在全球范围内，高分辨率的中新世火灾记录却很少。本文分析了青藏高原北部两个独立的以微炭为基础的火灾记录；两个记录都显示了微炭浓度随时间变化的相似趋势，在温暖的中中新世中期气候最适宜期（18-14 Ma）中丰度较低，随后在整个中新世晚期（14-5 Ma）冷期持续增加。详细的统计分析表明，微碳浓度的变化趋势与氧同位素（$\delta^{18}O$，r=0.94）和耐旱植物物种（$\%_{Xero}$，r=0.95）的变化趋势高度正相关。我们认为，青藏高原火灾频度的增加主要来源于森林-草原交错带，我们认为，青藏高原火灾频度的增加主要来源于森林-草原交错带，这是由于 18-5 Ma 期间全球降温和大气 pCO2 减少导致的冬季持续干旱，其次受青藏高原北部构造活动的控制。

ABSTRACT：Although fire is considered an important factor in global vegetation evolution and climate change, few high-resolution Miocene fire records have been obtained worldwide. Here, two independent micro-charcoal based fire records from the northern Tibetan Plateau were analyzed; both show similar trends in microcharcoal concentrations through time, with low abundances in the warmer Middle Miocene Climate Optimum (18-14 Ma) followed by a continuous increase throughout the late Miocene (14-5 Ma) cooling. Our detailed statistical analyses show that the micro-charcoal concentration trend is highly positively correlated to the trend in oxygen isotopes ($\delta^{18}O$, r =0.94) and xerophytic species ($\%_{Xero}$, r =0.95). We propose that the intensified fire frequency on the Tibetan Plateau mainly originated from the forest-steppe ecotone as a result of the continuous aridification in winter driven by the global cooling and decreased atmospheric pCO2 that occurred during 18-5 Ma, with a secondary control by the tectonic activity of the northern Tibetan Plateau.

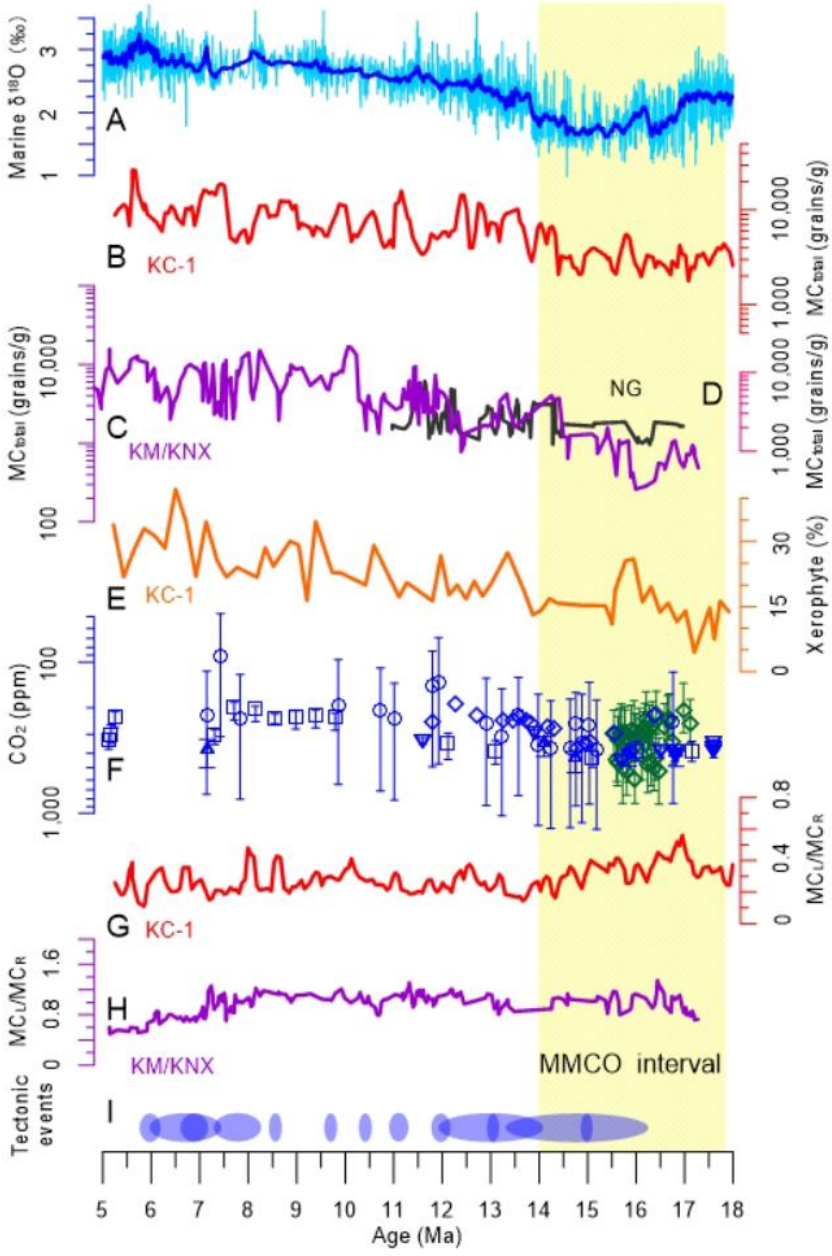

Figure 1. Data time series of climatic proxies and tectonic events on the northern Tibetan Plateau. MMCO-Middle Miocene Climate Optimum.A: Global deep-sea δ18O records (Zachos et al., 2001) (light blue) with 12-point averaging (darker blue). B–D: Micro-charcoal concentration (MC) records from KC-1 core, western Qaidam Basin (this study) (B), KM/KNX sections, Kumkol Basin (this study) (C), and NG section, eastern Qaidam Basin (Miao et al., 2016) (D). E: Xerophytic pollen percentages in KC-1 core (Miao et al., 2011). F: Synthesis of published pCO2 proxy data. Boron (diamonds) from Foster et al., 2012; Greenop et al., 2014. Stomata (inverted triangles) from Kürschner et al., 2008. Alkenone (regular triangles) from Zhang et al., 2013. B/Ca (squares) from Tripati et al., 2009. Paleosol (circles) from Ji et al., 2018. Error bars represent uncertainties in underlying assumptions of each proxy. G,H: Ratios of MCL/MCR (L—sub-long grains; R—sub-round grains) from KC-1 core and KM/KNX sections, respectively (this study). I: Tectonic events on the northern Tibetan Plateau (after Miao et al. [2012], Li et al. [2014], and Chang et al. [2015]). Curves in B–D and G–H are by three-point averaging.

8. 帕里西维拉盆地沉积物源演化---来自磁性地层学和矿物学的约束

翻译人：刘伟 inewway@163.com

Chunhui Xiao, et al. ***Constraints of magnetostratigraphic and mineralogical data on the provenance of sediments in the Parece Vela Basin of the western Pacific*** *[J].* ***Journal of Asian Earth Sciences****, 2020. doi.org/10.1016/j.jseaes.2020.104373*

摘要：通过对西太平洋帕里西维拉盆地 C-P19 岩心的磁性、矿物特征和古磁学年龄的分析，研究了西太平洋帕里西维拉盆地近 1Ma 年的沉积物源和沉积过程。结果表明，该孔的沉积下限年龄小于 1.072 Ma，沉积过程可分为两个阶段，约 1 ~ 0.78 Ma 期间沉积速率为 4.0 mm/kyr，0.78 Ma 之后沉积速率为 3.6 mm/kyr。这些沉积速率比周围地区小于 2 mm/kyr 的沉积速率要高。矿物特征和磁性参数表明从附近山脊侵蚀下来的火山物质被水流搬运到取样地点。这些火山沉积物是该区沉积物的主要来源，风成输入作用不大，非生物成因自生磁铁矿占部分磁性组分。近 1Ma 以来，沉积环境和沉积物物源发生了变化。997-880 ka 期间，火山活动增加，火山碎屑输入量大；880-443 ka 期间，沉积环境趋于稳定，沉积物供给减少。随着西太平洋火山活动的增加，沉积物输入量在约 443 ka 至今再次增加。

ABSTRACT: The sediment provenance and sedimentary processes of the Parece Vela Basin in the western Pacific during the last ca. 1 Myr were studied based on the analysis of magnetic properties, mineral features, and paleomagnetic ages of core C-P19. The results show that the sedimentary sequence has a lower limit age younger than 1.072 Ma, and the sedimentation process can be divided into two stages with sedimentation rates of 4.0 mm/kyr during ca. 1–0.78 Ma and 3.6 mm/kyr since 0.78 Ma. These sedimentation rates are higher than those in the surrounding area, where the sedimentation rate is generally less than 2 mm/kyr. Taken together with the mineral features and magnetic parameters, these findings show that volcanic sediments eroded from the nearby ridge were transported by currents to the sampling site. These volcanic sediments represent the main source of sediment in the area, with eolian inputs contributing little and nonbiogenic authigenic magnetite accounting for part of the magnetic fraction. The sedimentary environment and sediment provenance have varied during the last approximately 1 million years. During 997–880 ka, volcanic activity increased, and the input of volcanic clasts was high, whereas during 880–443 ka, the sedimentary environment tended to be stable, and the sediment supply decreased. With the increase

in volcanic activity in the western Pacific, the sediment input increased again during ca. 443 ka-present.

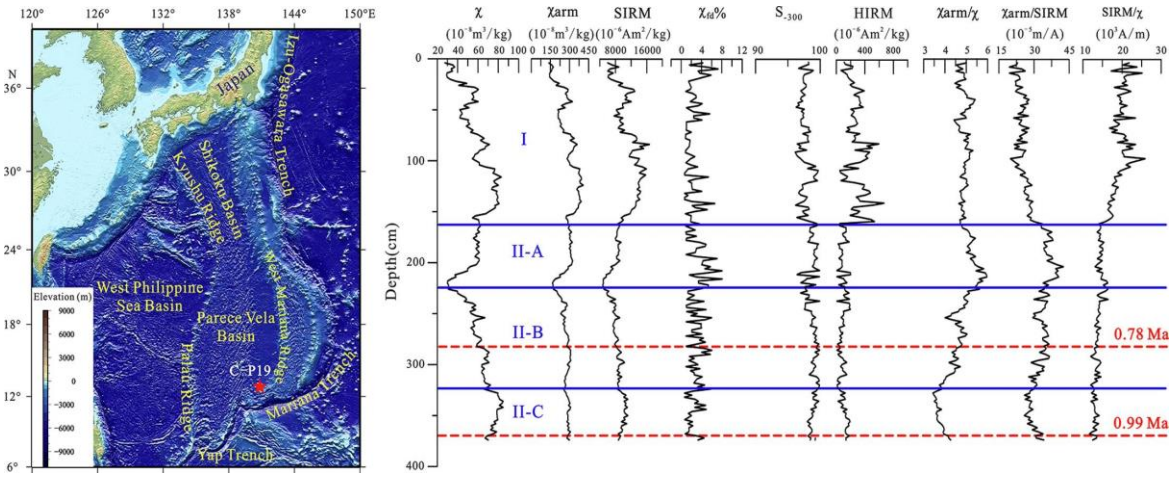

Figure 1. Variation in the environmental magnetic parameters with depth in the sediments of the C-P19 core.